

# CHEMISTRY

## A European Journal

A Journal of



### Accepted Article

**Title:** Polyfunctionalised nanoparticles bearing robust gadolinium surface units for high relaxivity performance in MRI

**Authors:** Chabloz Nicolas, Margot Wenzel, Hannah Perry, Il-Chul Yoon, Susannah Molisso, Graeme Stasiuk, Daniel Elson, Anthony Cass, and James Wilton-Ely

This manuscript has been accepted after peer review and appears as an Accepted Article online prior to editing, proofing, and formal publication of the final Version of Record (VoR). This work is currently citable by using the Digital Object Identifier (DOI) given below. The VoR will be published online in Early View as soon as possible and may be different to this Accepted Article as a result of editing. Readers should obtain the VoR from the journal website shown below when it is published to ensure accuracy of information. The authors are responsible for the content of this Accepted Article.

**To be cited as:** *Chem. Eur. J.* 10.1002/chem.201901820

**Link to VoR:** <http://dx.doi.org/10.1002/chem.201901820>

Supported by  
**ACES**

WILEY-VCH

## Polyfunctionalised nanoparticles bearing robust gadolinium surface units for high relaxivity performance in MRI

Nicolas G. Chabloz,<sup>[a]</sup>+ Margot N. Wenzel,<sup>[a]</sup>+ Hannah L. Perry,<sup>[a]</sup> Il-Chul Yoon,<sup>[a]</sup> Susannah Molisso,<sup>[a]</sup> Graeme J. Stasiuk,<sup>[b]</sup> Daniel S. Elson,<sup>[c]</sup> Anthony E. G. Cass,<sup>[a,d,e]</sup> and James D. E. T. Wilton-Ely\*<sup>[a,e]</sup>

[a] *Dr. N. G. Chabloz, Dr. M. N. Wenzel, H. L. Perry, I.-C. Yoon, S. Molisso, Prof. Dr. A. E. G. Cass, Prof. Dr. J. D. E. T. Wilton-Ely*  
*Department of Chemistry, Imperial College London,*  
*Molecular Sciences Research Hub, White City Campus, London W12 0BZ (UK).*  
*E-mail: j.wilton-ely@imperial.ac.uk*

[b] *Prof. Dr. G. Stasiuk*  
*School of Life Sciences, Biomedical Sciences, University of Hull, Hull HU6 7RX (UK)*

[c] *Prof. Dr. D. S. Elson*  
*Hamlyn Centre for Robotic Surgery, Institute of Global Health Innovation and*  
*Department of Surgery and Cancer, Imperial College London (UK)*

[d] *Prof. Dr. A. E. G. Cass*  
*Institute of Biomedical Engineering, Imperial College London (UK)*

[e] *Prof. Dr. J. D. E. T. Wilton-Ely, Prof. Dr. A. E. G. Cass*  
*London Centre for Nanotechnology (LCN)*

[+] *These authors contributed equally to this work*

### Keywords

Gold nanoparticles, gadolinium, dithiocarbamate, imaging, MRI

### Abstract

The first example of an octadentate gadolinium unit based on DO3A (hydration number  $q = 1$ ) with a dithiocarbamate tether has been designed and attached to the surface of gold nanoparticles (around 4.4 nm in diameter). In addition to the superior robustness of this attachment, the restricted rotation of the Gd complex on the nanoparticle surface leads to a dramatic increase in relaxivity ( $r_1$ ) from  $4.0 \text{ mM}^{-1} \text{ s}^{-1}$  in unbound form to  $34.3 \text{ mM}^{-1} \text{ s}^{-1}$  (at 10 MHz, 37 °C) and  $22 \pm 2 \text{ mM}^{-1} \text{ s}^{-1}$  (at 63.87 MHz, 25 °C) when immobilised on the surface. The ‘one-pot’ synthetic route provides a straightforward and versatile way of preparing a range of

multifunctional gold nanoparticles. The incorporation of additional surface units improving biocompatibility (PEG and thioglucose units) and targeting (folic acid) lead to little detrimental effect on the high relaxivity observed for these non-toxic multifunctional materials. In addition to the passive targeting attributed to gold nanoparticles, the inclusion of a unit capable of targeting the folate receptors overexpressed by cancer cells, such as HeLa cells, illustrates the potential of these assemblies.

## Introduction

Partly due to its benign biological reputation, metallic gold has been used extensively in medicine to address applications such as imaging,<sup>1</sup> therapy<sup>2</sup> and drug delivery,<sup>3</sup> including in clinical trials.<sup>4</sup> Gold nanoparticles (GNPs) are amongst the most studied, partly due to the control which can be exerted over their dimensions and partly due to the straightforward attachment of molecules to the surface through sulfur linkages (principally thiols). The thermal response to near-IR light irradiation of gold nanostructures is routinely employed in photothermal therapy (PTT) to induce apoptotic cell death.<sup>5</sup> Similar effects can also be achieved using photodynamic therapy (PDT), in which cytotoxic singlet oxygen / radicals are generated by the photoexcitation of suitable photosensitisers attached to the gold surface.<sup>6</sup> Furthermore, *in vivo*, even in the absence of functionalisation, gold nanoparticles accumulate at tumour sites (passive targeting) that have leaky, immature vasculature with wider fenestrations than normal mature blood vessels (enhanced permeability retention, EPR, effect).<sup>7</sup> For these reasons, GNPs are increasingly being employed in cancer therapy.<sup>8</sup>

In order to dramatically increase the selectivity of the targeting for certain cell types, additional surface units can be employed, such as aptamers (usually oligonucleotide or peptides) or antibodies.<sup>9</sup> GNPs bearing these aptamers have been shown to result in very specific protein binding, and this has been used to bring the nanostructure into the proximity of target proteins expressed by certain cells.<sup>10</sup> This targeting has been combined with photothermal therapy (PTT), in which irradiation of gold nanorods (GNR) leads to a temperature increase sufficient to cause destruction of the local environment.<sup>10</sup>

Magnetic resonance imaging (MRI) is a medical imaging technique that exploits the same principles as nuclear magnetic resonance (NMR) to acquire (non-invasively) detailed anatomical images that display the highest spatial resolution of all the imaging modalities. Different tissues possess a range of fundamental relaxation parameters (longitudinal relaxation

time,  $T_1$ ; transverse relaxation time,  $T_2$ ) and these parameters, in combination with proton density, govern contrast in MRI. This intrinsic contrast enables a detailed anatomical image to be acquired in MRI. Due to poor contrast between different tissue types (such as healthy and diseased), contrast agents can be used to accelerate the relaxation of local water protons in the surrounding tissue, improving the image detail. This can be achieved by the presence of an exogenous paramagnetic species, as  $T_1$  recovery and  $T_2$  decay are affected by the local magnetic moment. Higher relaxivity values (in  $\text{mM}^{-1} \text{s}^{-1}$ ) correlate with better contrast.<sup>11</sup> Most contrast agents used in a clinical setting (such as Dotarem<sup>®</sup>, Figure 1a) are based on paramagnetic ( $4f^7$ ) trivalent gadolinium ions, which interact with water molecules to improve the relaxation rates of the protons, enhancing the image contrast.<sup>11</sup> The attachment of Gd(III) units to the surface of gold nanoparticles has been shown previously to dramatically increase the relaxivity. This can be explained in terms of two parameters: Firstly, the rotational correlation time of the Gd(III) unit, which is greatly increased on binding to the nanoparticle surface. The nanoparticle assembly rotates more slowly than the unbound Gd(III) unit, leading to a rotational frequency closer in magnitude to the Larmor frequency and hence, enhanced relaxation rates.<sup>11</sup> Secondly, the degree to which the relaxation of water protons changes is due to the multimetric effect which stems from the increased, localised contrast agent concentration.<sup>11,12,13</sup> Many derivatives of DOTAREM have been used for this purpose, including DOTAGA, monoamido-DO3A (DOTMA) and DO3A.<sup>12c-e, 14</sup>

To date, all clinically-approved gadolinium MRI contrast agents (e.g., Dotarem<sup>®</sup>, Figure 1a) are extracellular probes with a non-specific biodistribution. Hence, the work presented here forms part of the next generation of contrast agents, which are able to recognise specific molecules on the cellular surface of diseased cells that act as early reporters of a given pathology. The targeting of overexpressed membrane receptors using MRI is hampered by the very low concentration of such receptors and by the relatively low sensitivity of Gd(III) contrast agents. To overcome this limitation, the approach used here is to accumulate a large number of imaging reporters (hundreds of Gd chelates) at the target site through active recognition by attached surface units (such as the folic acid used here).

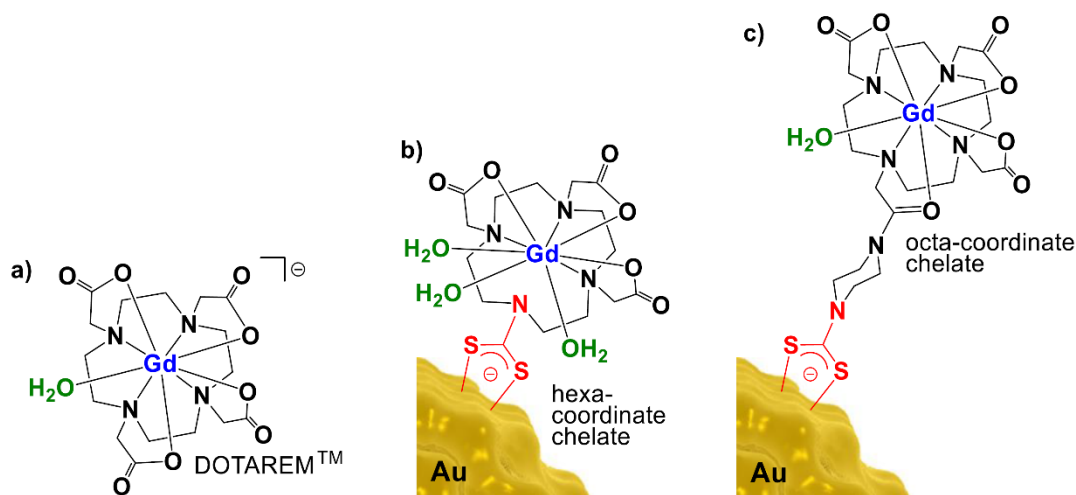


Figure 1. Design of a) clinically-approved contrast agent, Dotarem<sup>®</sup> ( $q = 1$ ), b) hexacoordinate Gd chelate ( $q = 3$ ) with a dithiocarbamate tether (shown in red), c) the octacoordinate Gd chelate ( $q = 1$ ) with a dithiocarbamate tether reported in this work.

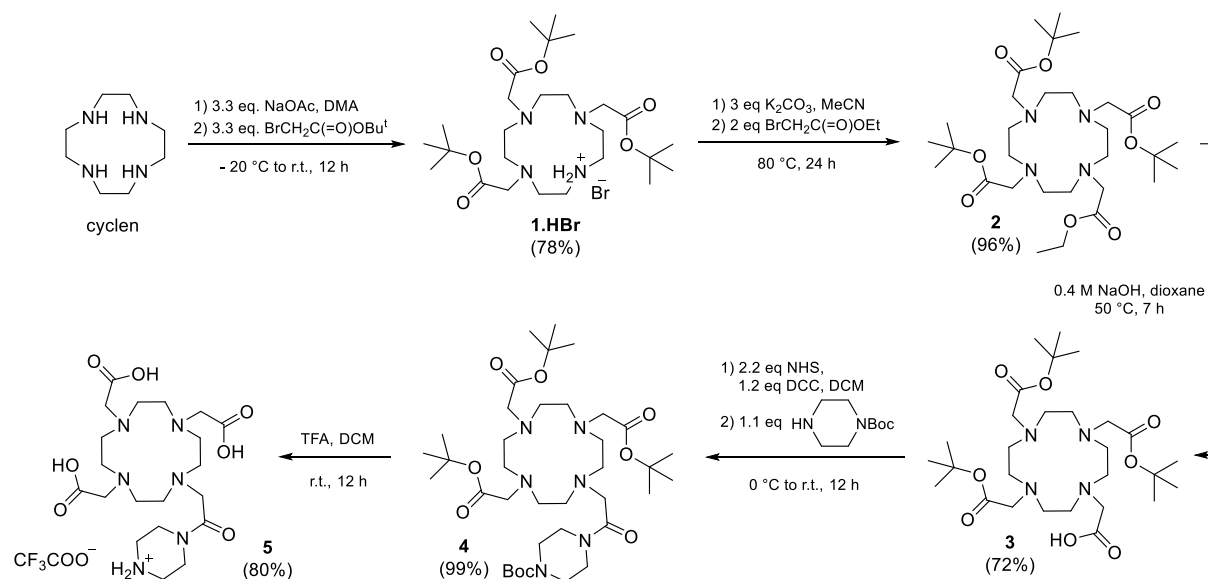
Since 2008, we have focused on the functionalisation of gold nanoparticles (GNPs) with transition metal units.<sup>14-18</sup> Much of this work has focused on the use of dithiocarbamate ( $R_2NCS_2^-$ ) tethers rather than the usual thiol(ate) or disulfide attachment methodologies. Competition experiments by us<sup>19</sup> and others<sup>20</sup> have shown that dithiocarbamates are able to displace thiol(ate)s from the surface of the nanoparticle, but not *vice versa*. Surprisingly, this robust attachment approach has still not been embraced widely with only relatively few examples of metals being tethered to GNPs in this way.<sup>21</sup> Theoretical investigations conducted using  $Au_{20}$  nanoclusters have provided an explanation for this more robust attachment.<sup>22</sup> They reveal much less distortion and reorganisation of the gold atoms compared to thiolates with no evidence of the ‘stapling’ effect observed structurally by Kornberg and co-workers in the crystal structure of  $Au_{102}(SC_6H_4CO_2H-4)_{44}$  nanoparticles (diameter 1.6 nm).<sup>23</sup> Stapling is the structural feature in which a gold atom is lifted out of the facet of gold atoms, potentially making it prone to loss as a molecular gold thiolate units.<sup>24</sup> Though often unacknowledged, attachment through a single thiol(ate) tether can lead to detachment of some of the units from the nanoparticle surface under physiological conditions. It is well established that the performance of the contrast agent can be dramatically enhanced by increasing the mass of the assembly through attachment to polymers, liposomes, nanoparticles or multimetallic (metallostar) arrangements.<sup>11</sup> This has been widely used in conjunction with various ways of reducing the freedom of rotation of the Gd(III) units to enhance the relaxation effect on the

protons of the water molecules. In 2014, we reported for the first time how dithiocarbamates could be used to attach gadolinium units to GNPs for potential use in MRI contrast enhancement.<sup>15</sup> These materials (Fig. 1b) showed promising relaxivity behaviour, however, the hexacoordinate coordination of the  $Gd^{3+}$  ion ( $q = 3$ ) raised concerns over the potential loss of this toxic ion under physiological conditions and so this was a major factor in the new design described based on an octadentate coordination environment (Fig. 1c), found in Dotarem<sup>®</sup> (Fig. 1a).<sup>25</sup>

This approach uses the most robust tether (dithiocarbamate) to attach the most critical surface unit, the imaging modality. Thiol(ate)s can then be used as an orthogonal methodology to introduce additional groups, providing biocompatibility and targeting. The straightforward synthesis combined with the versatility offered by modular design, gives access to a wide range of materials that can be used as a platform for multimodal imaging.

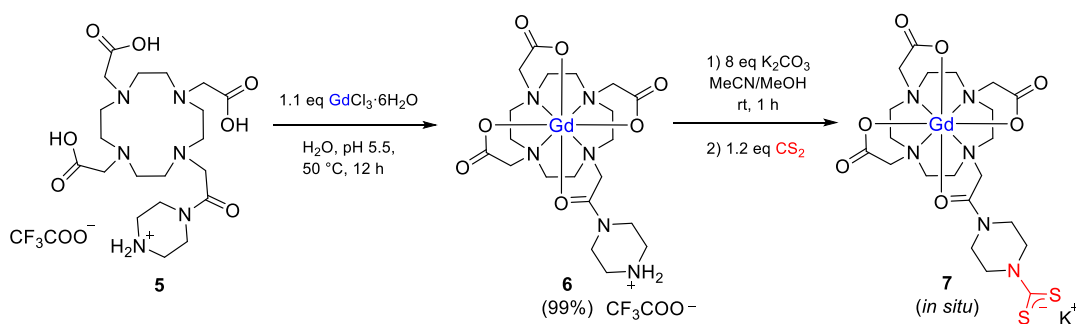
## Results and discussion

The new chelator **5** was prepared by a straightforward multi-step route (Scheme 1) starting from commercially-available cyclen via known intermediates **1**·HBr, **2** and **3**. All compounds, including previously unreported species (**4** and **5**), were fully characterized by <sup>1</sup>H, <sup>13</sup>C{<sup>1</sup>H} NMR and IR spectroscopy as well as high-resolution mass spectrometry (HR-MS) and elemental analysis.



Scheme 1. Synthesis of the new Gd chelator for anchoring to the GNPs.

Generation of the contrast agent was performed by addition of  $\text{GdCl}_3 \cdot 6\text{H}_2\text{O}$  to **5** (Scheme 2) followed by removal of any free (toxic) gadolinium ions (Xylenol orange test) as  $\text{Gd}(\text{OH})_3$ , precipitated under basic conditions. Infrared spectroscopic and mass spectrometry data were consistent with the formation of chelate **6**.



Scheme 2. Synthesis of **6** and the *in situ* conversion to dithiocarbamate-functionalised surface unit (**7**).

Compound **6** was found to be stable for months as a solid and could be prepared and stored on a large scale (> 1 g). Addition of  $\text{K}_2\text{CO}_3$  followed by carbon disulfide leads to the formation of the expected dithiocarbamate moiety (compound **7**), in line with our previous studies on piperazine-based dithiocarbamate complexes.<sup>16,17,26</sup> As discovered in these earlier studies, the long-term stability of **7**, both in solution and in the solid state, was found to be significantly worse than that of **6**, so compound **7** was always generated *in situ* when desired but not isolated. High-resolution mass spectrometry experiments nevertheless confirmed the generation of **7** ( $m/z$  702.1025). Furthermore, solid state infrared absorptions measured for **7** were attributed to  $\nu(\text{CN})$  and  $\nu(\text{CS})$  at  $1396\text{ cm}^{-1}$  and  $1002\text{ cm}^{-1}$ , respectively, providing evidence for the formation of the dithiocarbamate. This was reinforced by a resonance at 212.0 ppm in the  $^{13}\text{C}\{^1\text{H}\}$  NMR spectrum obtained for the diamagnetic lanthanum ( $\text{La}^{3+}$ ,  $f^0$ ) analogue of **7**, formed in an identical fashion.

Using a 0.25 T fast field cycling NMR relaxometer (see Supporting Information), the performance of **6** as an MRI contrast agent was established and compared to the current clinically-approved standard, Dotarem<sup>®</sup>. Compound **6** was found to possess a higher relaxivity than Dotarem<sup>®</sup>, perhaps due to the slightly higher molecular mass, which is known to enhance

relaxivity.<sup>11</sup> The Nuclear Magnetic Relaxation Dispersion (NMRD) profiles are shown in Figure 2. The presence of an amide arm on the chelates (as found in **6** and **7**) has been reported to potentially impact negatively on the relaxivity,<sup>27</sup> however, this does not seem to be a significant factor in the performance of the chelate design reported here.

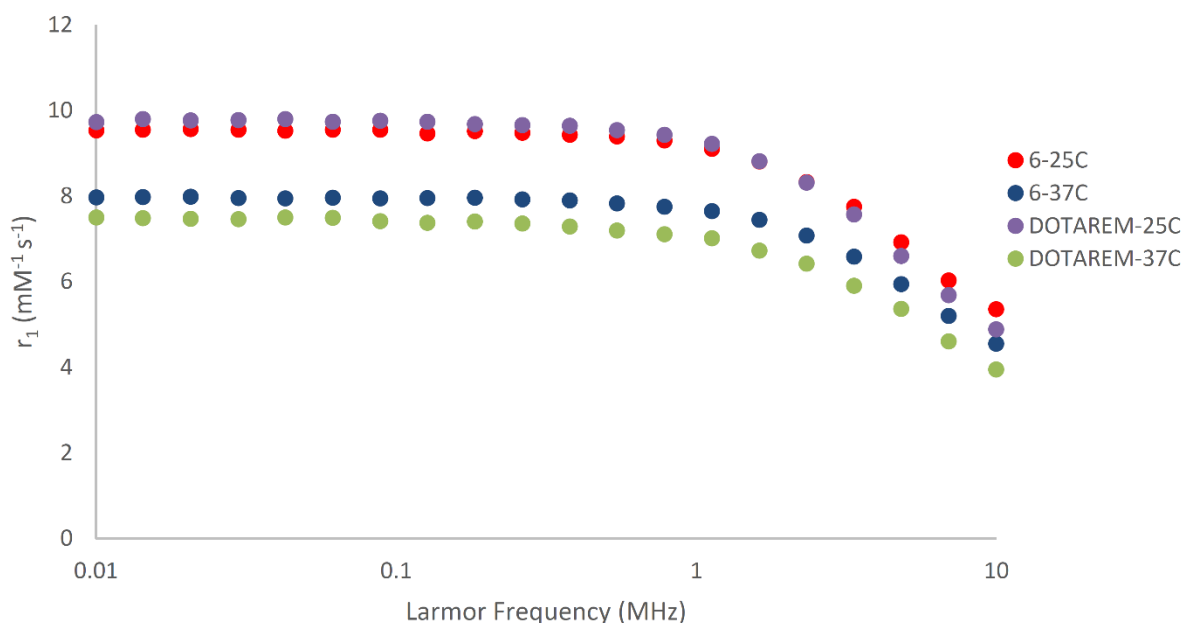


Figure 2. NMRD relaxivity profiles of **6** at 25 and 37 °C and Dotarem<sup>®</sup> under the same conditions.

The design of the chelator used to complex the gadolinium ion in **6** and **7** is intentionally closely based on that of Dotarem<sup>®</sup>, one of the leading clinically-approved contrast agents. The stability of the chelate towards loss of gadolinium ions (and hence its toxicity) was therefore expected to be comparable to the contrast agents used in the clinic. This was however probed by adding Zn<sup>2+</sup> ions to **6** and monitoring the relaxivity values obtained (Supporting Information), as described by standard literature protocols.<sup>28</sup> This revealed no change in the relaxivity even after 100 hours of exposure to 10 eq ZnCl<sub>2</sub> at 37 °C. Like Dotarem<sup>®</sup>, fluorescence lifetime measurements for the europium analogue (**8**) of compound **6** revealed the expected hydration value of  $q = 1$  for the octadentate chelate (Supporting Information). The assessment of the gadolinium surface unit was continued in cytotoxicity studies. MTT assays (HeLa cells, 24h incubation) were performed on **6** and showed no toxicity, even at



concentrations of 250  $\mu\text{M}$  (Supporting Information), which are even higher than those used clinically.

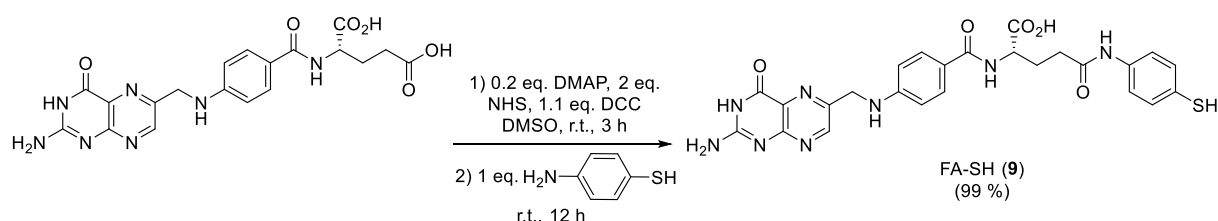
In addition to their stability under a range of physiological conditions, a great advantage of using gold nanoparticles is the ability to combine multiple groups on the surface.<sup>29</sup> Unlike other platforms, such as molecular systems or liposomes, new combinations of imaging/targeting/therapeutic units can be incorporated into assemblies of sizes 2-200 nm without fundamental changes to the design. Variables explored in this work include combinations of imaging unit (MRI and optical) and targeting alongside features to enhance biocompatibility/stealth. The overall aim was to design components which can be assembled in a straightforward manner to achieve a nanostructure with the appropriate functionality to target and image specific cell types (such as cancer cells).

Targeting groups (aptamers, antibodies etc.) can be chosen to recognise specific molecules on the cellular surface which act as early reporters of a given pathology. In a nanoparticle system such as the ones described here, the successful recognition of a receptor by a targeting group on the NP surface would lead to a high concentration of Gd chelates being present, compensating for the very low concentration of such receptors (e.g., overexpressed membrane receptors) and the relatively low innate sensitivity of Gd(III) contrast agents.<sup>30</sup>

As a proof of concept, folic acid was chosen to be added to the assembly to investigate uptake in HeLa cancer cells, which overexpress folate receptors on their surface.<sup>31</sup> This paves the way for more sophisticated and selective targeting units to be introduced in future studies, such as DNA/RNA aptamers and antibodies. In the case of tumours, the presence of active targeting groups would add to the passive targeting (EPR effect) already established for GNPs. This potential for conjugation of different thiol-based commercially-available targeting moieties, tailored to recognise specific proteins or disease sites, demonstrates the versatility of the proposed nanoparticles and their potential use as imaging platforms. The recognition moiety can be chosen based on the specific target and its intra- or extracellular location.

Folic acid (FA) is known to provide additional targeting of nanoparticles beyond the tendency for GNPs to accumulate in tumours through the EPR effect, enhancing the uptake in

cells.<sup>7</sup> A thiol-terminated derivative, FA-SH (**9**), shown in Scheme 3, was prepared using a modified procedure,<sup>32a</sup> which avoids compromising the recognition function of the molecule.<sup>32</sup>



Scheme 3. Synthesis of a targeting surface unit, FA-SH (**9**), derived from folic acid.<sup>32a</sup>

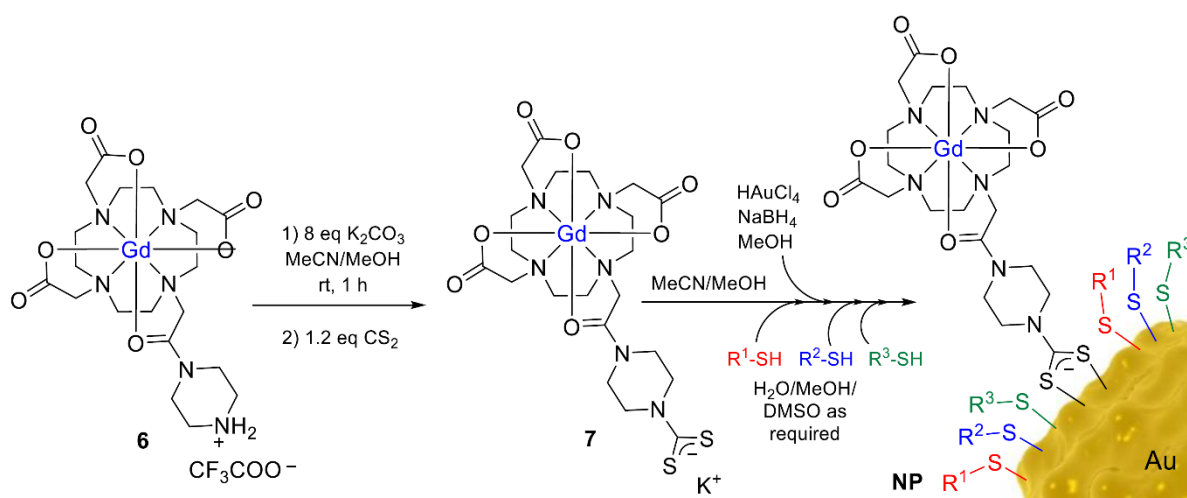
Two further surface units, PEG-SH and thioglucose were used to enhance the functionality of the surface architecture. Poly(ethylene)glycol (PEG) units are well established units used to enhance biocompatibility, while thioglucose has been suggested to perform a targeting function (due to the higher consumption of glucose by tumours)<sup>33</sup> as well as conferring water solubility.<sup>34</sup>

Gold nanoparticles can be imaged using their interaction with light (fluorescence) and this will allow their location and uptake to be visualised in cells. As this fluorescence is weak (quantum yields ~0.3%), a thiol-terminated boron-dipyrromethene (BODIPY-SH) fluorophore (**12**, Supporting Information), similar to the type used extensively in biological imaging,<sup>35</sup> was also attached to the surface of the nanostructures to study their uptake.

Early work in the area<sup>30,36</sup> employed thiol precursors to attach Gd chelates to the surface of gold nanoparticles (GNPs),<sup>37</sup> however there is evidence to indicate loss of thiolates from the GNP surface occurs to a substantial degree.<sup>21,38</sup> This led us to explore a more robust attachment for the Gd unit, resulting in the design of compound **7**. The dithiocarbamate unit combines superior strength of attachment (compared to thiol(ate)s)<sup>20,21,38-40</sup> with limited rotational freedom to maximise the relaxivity ‘boost’ obtained on immobilising the Gd chelate on the nanoparticle. In addition, its similarity to a clinically-approved design (Dotarem<sup>®</sup>), enhances the likelihood of showing similar biological properties.

A general protocol for the synthesis of gold nanoparticles (Scheme 4) was formulated based on the Brust-Schiffrin method.<sup>41</sup> All glassware used for the synthesis of GNPs was washed with *aqua regia* and rinsed thoroughly beforehand to remove any residues. A methanol

solution of tetrachloroauric acid was prepared and solutions of the various sulfur-based ligands (**7**, PEG-SH, thioglucose, FA-SH (**9**), BODIPY-SH (**12**)) were then introduced in the desired quantities and ratios (0.01 - 1 eq. relative to Au). Ultrapure water was used to dissolve PEG-SH and thioglucose, DMSO for BODIPY-SH (**12**), and a 1:1 mixture of ultrapure water and DMSO for FA-SH (**9**) and a 1:1 mixture of methanol and acetonitrile for **7**. The mixture was then cooled to 4 °C and a fresh solution of sodium borohydride in ultrapure water added dropwise to reduce the Au(III) precursor to Au(0). The mixture was stirred at 10 °C for 3 hours, after which the nanoparticles were then centrifuged at 5300 rpm for 45 minutes. The supernatant was removed and the nanoparticles were repeatedly rinsed with ultrapure water a minimum of 3 times, until the filtrate failed to show the presence of the unbound Gd chelate (**7**), as determined by measurement of its relaxivity. The nanoparticles were then resuspended in ultrapure water and stored in this form. Indeed, even after 6 months, the functionalised nanoparticles could be re-suspended and their relaxivity measured. This revealed no changes in their performance and indicate their long-term stability.



Scheme 4. Synthesis of GNPs with **7** and other surface units ( $R^1-SH$ ,  $R^2-SH$ ,  $R^3-SH$ ).

A total of 7 types of functionalised GNPs were prepared with different surface units and the ratios of the components used are shown in Figure 3.

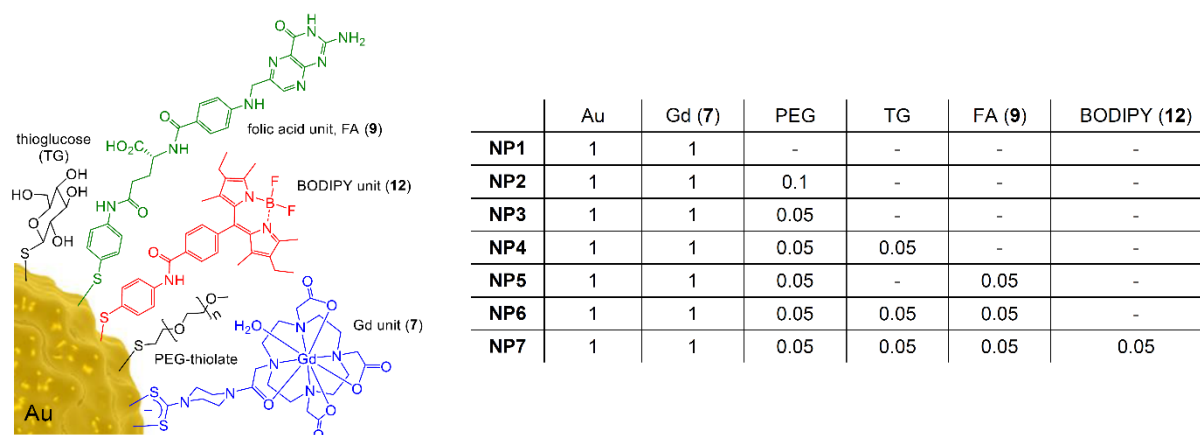


Figure 3. Nanoparticle surface functionalization with proportions of surface units used.

This approach represents a rapid and straightforward route to the preparation of multifunctionalised gold nanoparticles in which the greater strength of attachment (compared to thiolates) of the DTC unit (7) ensures the retention of the Gd contrast agent. Transmission electron microscopy (TEM) was used to determine the diameter and size distribution of the nanoparticles (Figure 4). A reasonably narrow size distribution was found with the nanoparticles being around 4.4 nm in diameter (ranging from 4.18 – 4.55 nm). Dynamic light scattering (DLS) measurements for the PEGylated NPs suggested that the hydrodynamic radius increases from 4-5 nm to approximately 20 nm due to the PEGylated thiolate surface units (PEG-2000). Dispersive X-ray spectroscopy (EDS) was used to confirm the presence of Gd and Au in the assemblies (Figure 4). The ratio of Gd and Au was more accurately determined by inductively-coupled plasma optical emission spectroscopy (ICP-OES) and allowed the number of Gd chelates per GNP to be calculated and this was used for relaxivity measurements. These data were compared to thermogravimetric analysis (TGA) for **NP1** (bearing just 7 on the surface) and found to be in good agreement. For **NP1** it was calculated<sup>42</sup> from TEM and ICP-OES data that there are approximately 120 Gd chelates per nanoparticle. As no other surface units are present, this can be assumed to be close to the maximum possible loading of Gd units for this diameter of nanoparticle.

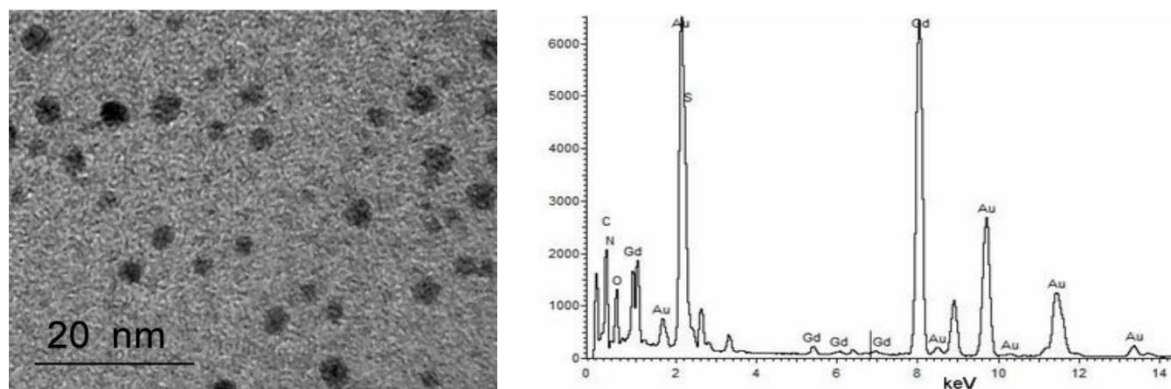


Figure 4. TEM (left) and EDS (right) data for **NP1**.

It is well established that the addition of PEG-SH units improves the solubility of GNPs in biological media, enhances biocompatibility and performs a ‘stealth’ function,<sup>43</sup> which would be important in any clinical application as it prevents removal by the body’s defences (e.g. macrophages). Using an adapted procedure (Scheme 4) to that employed for the synthesis of **NP1**, nanoparticles (**NP2** and **NP3**) with mixed surface units were prepared, using different ratios of PEG-SH and the Gd chelate (**7**). Nanoparticles functionalised with more than two surface units (**NP4** - **NP7**) were synthesised using only 0.05 mole equivalents of PEG as **NP2** was visibly less stable than **NP3** after 3 weeks of storage.

In addition to **7**, thioglucose was also added in equimolar amounts to PEG-SH to generate **NP4**, which resulted in a triply functionalised surface. Despite the overlapping bands from the various surface units, which have many functional groups in common, analysis of the infrared spectroscopic data indicated the presence of an absorption band at around  $1237\text{ cm}^{-1}$ , which was assigned to thioglucose.

Two further assemblies (**NP5** and **NP6**) were functionalised with the thiol-modified derivative of folic acid (FA-SH, **9**), differing only in the Gd : FA-SH ratio (Figure 3). **NP6** was prepared in order to demonstrate that four separate surface units (Gd, PEG, TG and FA) could be combined on the surface of the nanoparticle without a significant compromise in the relaxivity performance. The final nanoparticle assembly (**NP7**) included a BODIPY (**12**) unit to aid tracking of the assembly using fluorescence (*vide infra*). Thermogravimetric analysis (TGA) performed on **NP2** – **NP7** indicated that between 20 and 34% of the mass of the nanoparticles was due to the surface units, however, due to the sensitivity of the technique, exact quantification of each surface unit was not possible.

Electronic spectroscopy (UV-vis) was used to observe the surface plasmon resonance (SPR) band for each assembly (at approximately 550 nm). For each nanoparticle, zeta potential measurements were carried out to provide information on the stability of the nanoparticles towards agglomeration. These ranged between  $-30.4$  and  $-35.8$  mV (Supporting Information), indicating good stability and resistance to agglomeration.

The nanoparticles were also found to be stable for at least 24 hours across a range of pH values between 4 – 10 (HEPES buffer solution). The stability in the presence of NaCl was tested in water and monitored by UV-vis spectroscopy, showing no tendency to precipitate over a period of 24 hours. The same technique was used to analyse their behaviour in biological media, which revealed no changes to the data. See Supporting Information for further details.

The relaxivity of the various nanoparticle assemblies was measured at 37 °C in water and NMRD profiles were determined. It is known that the immobilisation of gadolinium chelates on a polymer or nanoparticle surface often results in an enhancement of the relaxivity.<sup>11,45</sup> This is due to slow tumbling and a reduction in the rotational freedom experienced by each individual Gd chelate. However, a particularly pronounced enhancement was observed for the materials prepared in this study (up to five times higher relaxivity per Gd). This can partly be attributed to the particularly rigid design of **7**, which has multiple bond character in the C-N bonds of both the dithiocarbamate and amide linkages. A representative NMRD profile is shown below (Figure 5). Previous designs based on thiol-modified chelates allow rotation about the axis of the tether<sup>30,34,36,37,44</sup> or can lead to the formation of disulfide linkages, creating flexible chains of Gd chelates anchored at only a few points to the surface.<sup>36a</sup> For example, many reports use long PEG-thiolate chains terminated in a Gd unit, which retain their internal flexibility and this restricts the enhancement observed. (Scheme S2-1 in ESI).<sup>44</sup> These effects potentially reduce the benefit of immobilisation on the nanoparticle surface and are sometimes overlooked due to the tendency to quote relaxivity per nanoparticle rather than per Gd.

Nanoparticles with only Gd surface units (**NP1**) show good water solubility and were found to exhibit an 8-fold enhancement over the unattached surface unit **6** (from  $4.0 \text{ mM}^{-1} \text{ s}^{-1}$  to  $34.3 \text{ mM}^{-1} \text{ s}^{-1}$  at 10 MHz, 37 °C).

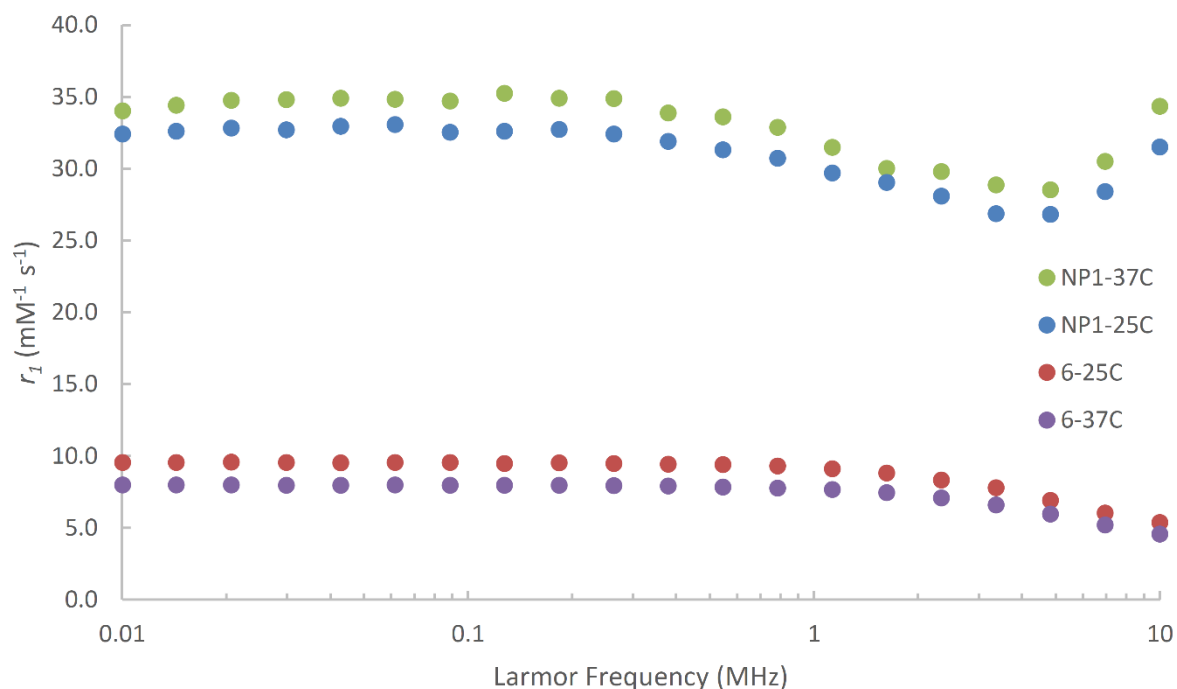


Figure 5. NMRD profiles of **NP1** and **6**.

The relaxivity performance of **NP1** exemplifies the effect of immobilising the Gd chelates on the nanoparticles. These nanoparticle-bound chelates displayed a dramatic relaxivity enhancement (7.6 times greater for **NP1**) compared to that of non-immobilised **6**, as can be seen from the NMRD profiles shown in Figure 5 and Table 1. For **NP1**, relaxivities of  $r_1 = 34.3 \text{ mM}^{-1} \text{ s}^{-1}$  per Gd and  $r_1 = 4203 \text{ mM}^{-1} \text{ s}^{-1}$  per nanoparticle were achieved (at 10 MHz, 37 °C). This represents the highest relaxivity enhancement per Gd ion yet reported for small spherical gold nanoparticles that could potentially be used in a clinical setting. A slightly higher value ( $r_1 \sim 40 \text{ mM}^{-1} \text{ s}^{-1}$  at 10 MHz, 37 °C) was reported by Helm and co-workers<sup>36b</sup> for gold nanoparticles with a surface unit based on a heptadentate chelate with a hydration number of two. The authors suggest that this design would be suitable for pre-clinical but not clinical imaging (on account of nephrogenic systemic fibrosis concerns), due to the lower stability of the chelate. This performance of **NP1** can be attributed to the internal rigidity of the Gd surface unit provided by the multiple bond character present at either end of the dithiocarbamate linker (in both DTC and amide units). The lack of rigidity within the Gd surface unit and tether has been identified<sup>45</sup> as the main factor limiting the relaxivity enhancement in gold nanoparticles functionalised with molecular Gd units (Scheme S2-1 in ESI).

The relaxivity of simple, monometallic Gd-based contrast agents is severely affected by the short rotational correlation time. An increase in temperature causes more rapid tumbling and so decreases  $r_1$  values still further despite the higher water exchange rate at elevated temperatures. In current designs based on Gd chelates attached to nanoparticles,<sup>13,36,37,44</sup> slower tumbling is achieved but internal rotation (e.g. about the tether) limits the enhancement through this effect. Due to the rigidity introduced into our system by the dithiocarbamate, an increase in temperature has little impact on the rotation of the Gd surface unit (**7**), while still allowing the beneficial effects of a higher water exchange rate. This can be seen in Figure 6, which plots the relaxation rate ( $R_1$ ) at temperatures between 30 – 70 °C over the value at 30 °C (at 7 MHz) for monometallic **6** and **NP1**. This reveals the expected decrease in values for **6**, whereas the corresponding experiments for **NP1** lead to an increase in relaxation rate.

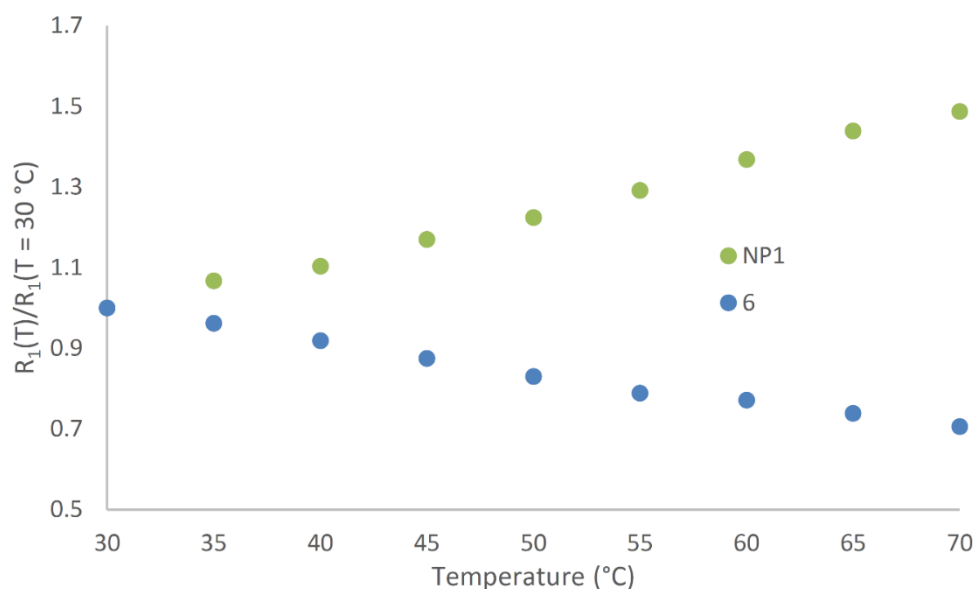


Figure 6. Plot of the ratio of relaxation rate ( $R_1$ ) at temperatures between 30 – 70 °C relative to the value at 30 °C (at 7 MHz) for monometallic **6** and **NP1**.

The GNPs functionalised with PEG-SH units (**NP2** and **NP3**) showed a slightly reduced relaxivity per Gd compared to **NP1** possibly due to crowding of the Gd chelates by the PEG units, reducing their exposure to the bulk water (Table 1).

Relaxivity data were also recorded for **NP2** – **NP7** in order to explain the effect of adding further groups to the GNP surface. Increasing the complexity of the surface architecture does have some impact on the relaxivity per Gd centre (Figure 7 and Figure S8-8 in the Supporting Information), however, the overall enhancement compared to Dotarem<sup>®</sup> or



compound **6** is still substantial. The reduction in relaxivity per Gd observed could be due to a number of factors. The presence of the substantially longer and more flexible PEG units could hinder water coordination, exchange and outer sphere relaxation effects, while the lower density of Gd chelates would reduce the likelihood of enhanced relaxivity through the cooperative action of neighbouring Gd chelates. Interestingly, the presence of thioglucose seems to enhance the relaxivity, as has been noted previously.<sup>34,46</sup> This could be due to the small size of the thioglucose units relieving the crowding of the Gd chelates caused by the much longer and more flexible PEG units, thus allowing better interaction with the bulk water.

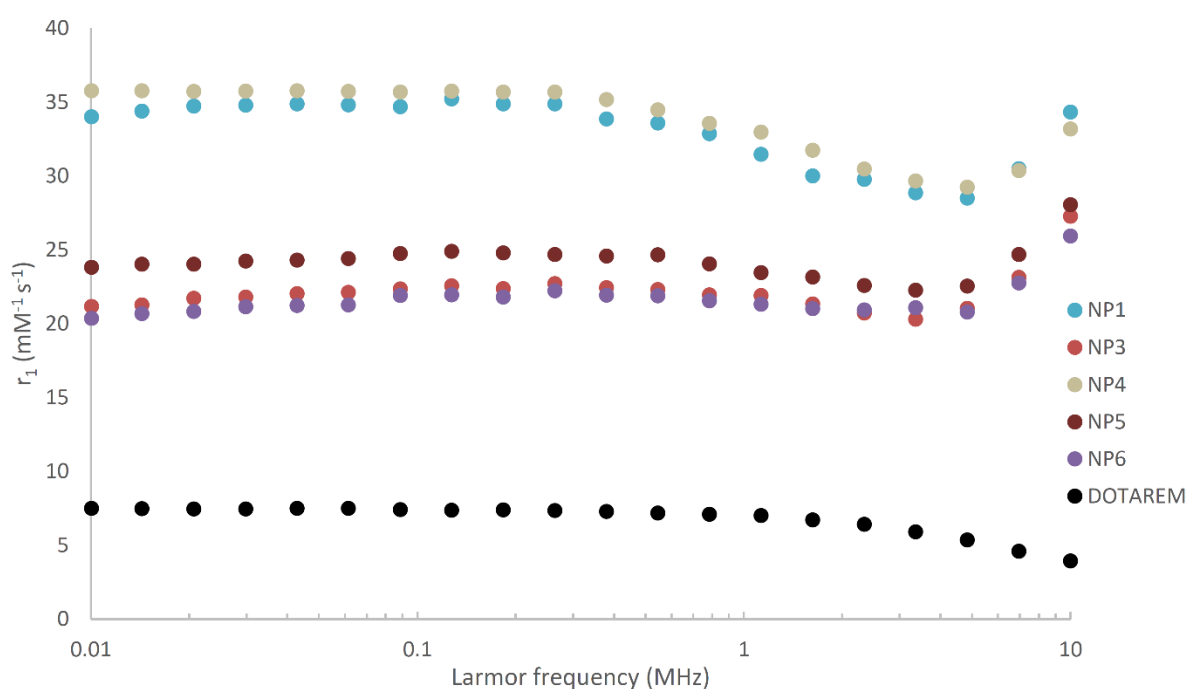


Figure 7. NMRD profiles (*per Gd*) for the nanoparticles at 37 °C.

The use of additional surface units for other functions (biocompatibility, targeting, therapy etc.) should lead to an overall reduction in relaxivity per nanoparticle due to fewer Gd chelates being present on the nanoparticle surface. This is evident in Figure 8 and Table 1, with **NP6** (containing 3 additional surface units) showing the lowest relaxivity per nanoparticle.

Table 1. Summary of the relaxivity values ( $\text{mM}^{-1} \text{s}^{-1}$ ) for the various GNPs measured at 25 and 37 °C at 10 MHz and the number of Gd units per nanoparticles (from TEM and ICP-OES data).

	Number of Gd per GNP	25 °C		37 °C	
		$r_1$ per Gd	$r_1$ per GNP	$r_1$ per Gd	$r_1$ per GNP
NP1	122	31.49	3855	34.34	4203
NP3	89	20.63	1830	27.27	2423
NP4	75	34.94	2605	33.19	2473
NP5	86	26.13	2256	28.06	2423
NP6	82	22.39	1831	25.94	2120
<b>6</b>	-	5.34	-	4.54	-
Dotarem <sup>®</sup>	-	4.89	-	3.94	-

The overall  $r_1$  value per nanoparticle (TEM: around 4.4 nm in diameter) decreases from 4203  $\text{mM}^{-1} \text{s}^{-1}$  for **NP1** (Gd only, at 10 MHz, 37 °C) to 2120  $\text{mM}^{-1} \text{s}^{-1}$  for **NP6** (at 10 MHz, 37 °C) due to the lower loading of Gd chelates on the surface. However, the localised impact of this large relaxation effect will still be substantial and should lead to a great contrast enhancement compared to the diffuse and non-localised effect of monometallic species such as Dotarem<sup>®</sup>. Indeed, if the targeting moieties on the nanoparticle were to bring such a high payload of Gd into the vicinity of a receptor expressed by a tumour, the contrast enhancement observed would be much greater as a result of this single receptor compared to a targeting unit linked to one or only a few Gd centres. In addition to their high localised relaxivity, the small sizes of the nanoparticles described here allow them to penetrate membranes more easily than larger nanostructures. However, if larger GNPs are required, the approach described here can also be applied to generate larger functionalised nanostructures.

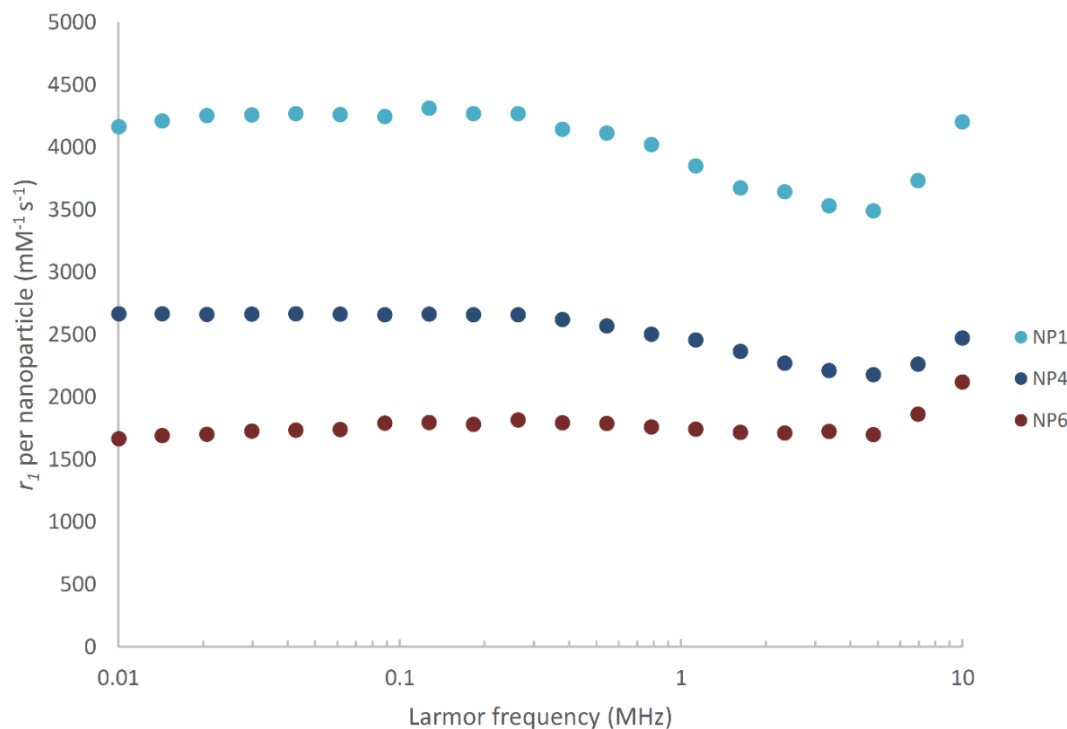


Figure 8. NMRD profiles for three representative nanoparticles in the study (NP1, NP4, NP6) as measured *per nanoparticle* at 37 °C.

The GNPs were tested for their effect on various cell lines using MTT assays. They were found not to be cytotoxic towards the cell lines tested (HeLa, MCF-7) at concentrations up to 250  $\mu\text{M}$  (Supporting Information).

Measurement of GNP uptake (HeLa and MCF-7) was determined after incubation for 24 hours with the differently functionalised GNPs. HeLa and MCF-7 cell lines were chosen due to their differing expression of the folate receptor (higher in HeLa).<sup>47</sup>

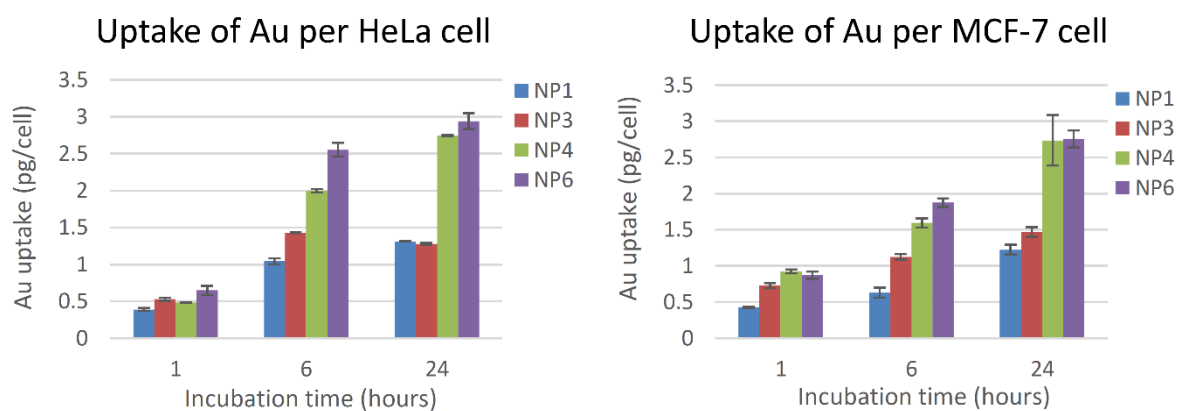


Figure 9. ICP-OES experiments measuring the uptake of gold (in pg/cell) in HeLa (left) and MCF-7 (right) cells over various incubation times.

The data in Figure 9 show that the more highly functionalised nanoparticles display greater uptake after 6 and 24 hours than the materials with only Gd surface units (**NP1**) or Gd and PEG units (**NP3**). HeLa cells express the folate receptor to a greater extent than MCF-7 cells<sup>47</sup> and this could explain the enhanced uptake of **NP6** (particularly after 6h), which is the only assembly functionalised with folic acid. However, it is likely that the uptake observed is not solely due to the presence of the folic acid group as **NP4** (bearing thioglucose but not folic acid) also shows increased uptake. Further studies will be conducted to investigate the uptake mechanism in more detail, including using unbound folic acid as part of a competition study. In future research, it is likely to be beneficial to exchange folic acid for a nucleic acid aptamer, which is capable of binding to its target with high affinity and specificity.<sup>48</sup>

Widefield microscopy (FILM, Imperial College) was used to show (in HeLa cells), that the GNPs enter the cells but apparently not the nucleus (Figure 10). This was determined using BODIPY-functionalised nanoparticles. When characterised, these nanoparticles showed quenching of the BODIPY fluorescence (heavy atom effect) by the gold nanoparticle due to the short length of the tether. This is in accordance with previous studies on the effect of tether length on quenching.<sup>49</sup> However the fluorescence is observed after one hour of incubation in the microscopy images (predominantly inside the cells, which supports the ICP-OES data for cell uptake), suggesting that the BODIPY unit (**12**) has detached from the nanoparticle surface, leading to revival of the fluorescence. This can be taken as further evidence for the loss of some of the thiolate units from the surface under biological conditions,<sup>39e</sup> reinforcing the need for robust attachment of the principal imaging unit – the Gd chelate.

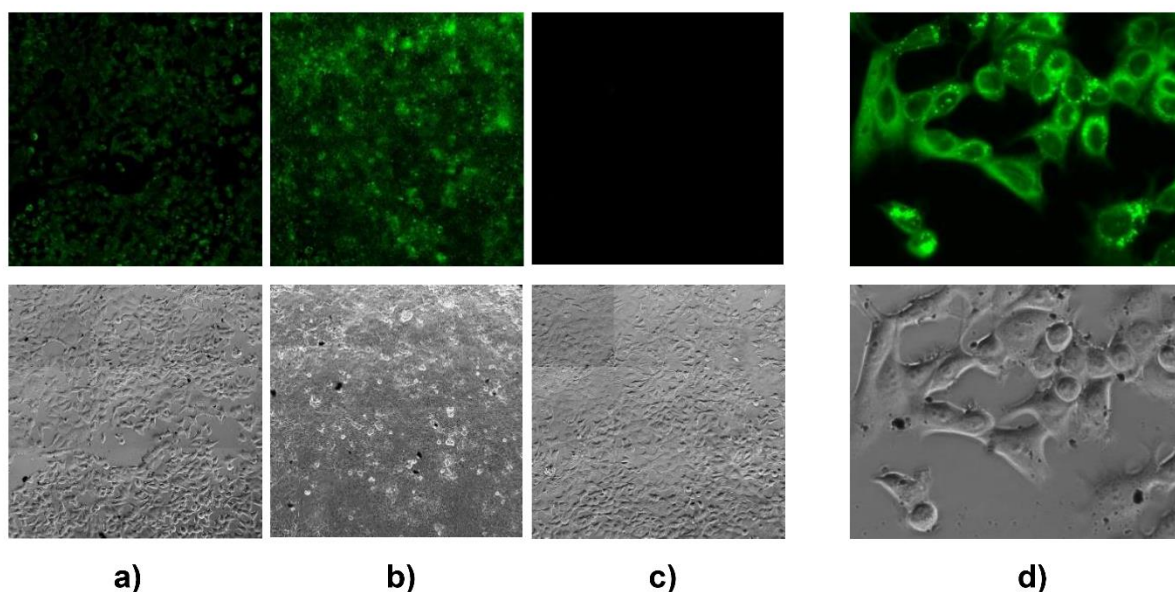


Figure 10. Widefield images (fluorescence above and brightfield below) showing fluorescence due to release of the BODIPY-thiolate surface unit (**12**) from **NP7** ( $[\text{Au}] = 200 \mu\text{M}$ ) after a) 1 h incubation, b) 24 h incubation, c) control with no GNP and d) a close up of cells after 24 h incubation. Excitation at 450 nm.

The  $T_1$ -weighted MR images of the nanoparticles shown in Figure 11 were measured on a clinical scanner at 63.87 MHz (1.5 T) and compared to Dotarem<sup>®</sup>. This reveals that for the same concentration of  $\text{Gd}^{3+}$  ions (0.02 mM), significantly greater contrast can be achieved per  $\text{Gd}^{3+}$  unit in **NP1** ( $r_1 = 22 \pm 2 \text{ mM}^{-1}\text{s}^{-1}$ ) and **NP6** ( $r_1 = 14 \pm 1 \text{ mM}^{-1}\text{s}^{-1}$ ) compared to Dotarem<sup>®</sup> ( $r_1 = 4.5 \pm 0.3 \text{ mM}^{-1} \text{ s}^{-1}$ ). As expected, and in agreement with previous reports on other gold nanoparticle-based contrast agents,<sup>12</sup> there is a reduction of relaxivity at the higher frequency used by clinical scanners compared to at 10 MHz (**NP1**,  $r_1 = 31.49 \text{ mM}^{-1}\text{s}^{-1}$ ; **NP6**,  $r_1 = 22.39 \text{ mM}^{-1}\text{s}^{-1}$ ).

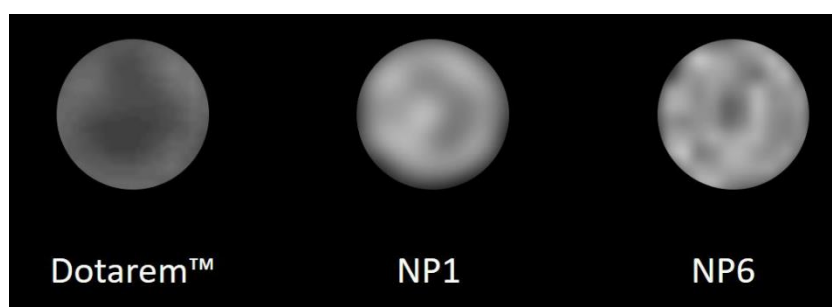


Figure 11.  $T_1$ -weighted MR images of Dotarem<sup>®</sup>, **NP1** and **NP6** at 25 °C at 63.87 MHz (1.5 T).  $[\text{Gd}^{3+}] = 0.02 \text{ mM}$ . Modified Look-Locker Imaging (MOLLI)  $T_1$  sequence.

The approximately 3.5x and 4.8x increase in relaxivity per Gd of both **NP1** and **NP6**, respectively, at clinical field compared to Dotarem<sup>®</sup>, combined with their biocompatibility and increased cellular uptake, makes these nanomaterials suitable for use in high-field MRI scans.

## Conclusions

Many strategies have been employed to enhance the relaxivity offered by trivalent gadolinium chelates for use in MRI<sup>11,45</sup> and one of the most successful is their immobilisation on the surface of gold nanoparticles. Alongside the advantages, such as slow tumbling and passive targeting, drawbacks associated with thiolate tethers need to be avoided, such as the formation of undesirable disulfide bonds and the internal flexibility (and rotation about) the tether. As a solution to these limitations, this contribution describes the multigram synthesis of a new octadentate gadolinium chelate (**7**) based on the clinically-approved DOTA scaffold ( $q = 1$ ) with a rigid tether. This piperazine-based unit prevents rotation due to the multiple bond character in the amide moiety at one end and through the robust, dithiocarbamate anchor at the other. Furthermore, this attachment at two points on the gold surface through the two sulfur atoms of the dithiocarbamate avoids the rotation permitted by the single Au-S interaction of thiolate surface units. This is the first time a dithiocarbamate has been used to generate nanoparticles bearing Gd chelates (with  $q = 1$ ) that are suitable for use in MRI, following our previous report of a dithiocarbamate-functionalised hexadentate chelate ( $q = 3$ ).<sup>15</sup> A relaxivity enhancement per Gd of up to 8 times is observed compared to unattached **6** (at 10 MHz) and the overall assembly displays  $r_1$  values of around 4200 mM<sup>-1</sup> s<sup>-1</sup> per nanoparticle. Under clinical conditions (1.5 T, 63.87 MHz), enhancements per Gd of 3.5 - 4.8x compared to Dotarem<sup>®</sup> are observed. In contrast to monometallic (e.g., Dotarem<sup>®</sup>) or Gd chelates immobilised on nanoparticles or polymers where internal rotation is possible, an increase in temperature (as observed between 25 and 37 °C) results in an enhancement of the measured  $r_1$  values and this is attributed to the combination of the rigidity in our system and the improved water exchange at elevated temperatures. Given that pathologies, such as tumours, typically express only a few receptors, the targeting of these receptors with a large payload of Gd chelates will help locate diseased tissue through a vastly improved MRI signal. The use of the dithiocarbamate surface unit to attach the most valuable component (MRI modality) of the surface architecture both ensures superior robustness (compared to monothiolate attachment) and allows thiol(ate)s to

be used in an orthogonal approach to creating mixed surfaces. In our work, this has been exploited to provide a straightforward and versatile ‘one-pot’ synthetic approach to generate multifunctional nanoparticles with up to four other surface units to add biocompatibility (PEG-SH), targeting (FA-SH), uptake (thioglucose) and optical imaging (BODIPY-SH) properties. As well as being non-toxic, the resulting nanoparticles show very good stability (Supporting Information) when tested under different pH conditions, high salt concentrations and for potential transmetallation (with  $Zn^{2+}$  ions). In addition to the passive targeting attributed to gold nanoparticles (EPR effect), the inclusion of a unit capable of selectively targeting overexpressed receptors in cancer cells illustrates the potential of these assemblies. The small size of the nanoparticles is also suited to relatively short circulation times and good clearance properties.

Our current investigations focus on combining the enhanced magnetic resonance imaging properties of these materials with therapeutic options. Potentially, this will allow functionalised nanoparticles to be used to both evaluate disease progression and deliver therapeutic interventions. The work described here has provided a new methodology for functionalising nanoparticles using highly stable Gd chelates with a dithiocarbamate tether. This approach has the potential to generate functionalised GNPs, which can deliver targeted imaging agents.

### Supporting Information

The synthesis and subsequent characterization of the functionalised nanoparticles are described in the ESI along with details of cytotoxicity and cell uptake studies.

### Acknowledgements

The authors wish to express their gratitude to the Wellcome Trust for the Networks of Excellence Award (to M. N. W.) and to the EPSRC for a DTP studentship (to N. G. C.). The EPSRC Centre for Doctoral Training in Medical Imaging (King’s College London and Imperial College London) is acknowledged for provision of relaxometer and MRI (St. Thomas’ Hospital) facilities and funding (to H. L. P.). The award of a President’s PhD Scholarship is gratefully acknowledged (I.-C. Y.). Mr Andrew Coulson is thanked for assistance with tissue culture facilities. We are grateful for the assistance of Dr Ecaterina Ware in obtaining the TEM images and Ms Patricia Carry for ICP-OES facilities. Prof. René Botnar is gratefully acknowledged for the provision of access to a clinical scanner and Giovanna Nordio is thanked

for the measurement of the scanner data. We thank the Facility for Imaging by Light Microscopy (FILM) for access to microscopy instruments. This facility is supported by funding from the Wellcome Trust (grant 104931/Z/14/Z) and BBSRC (grant BB/L015129/1).

## References

1. Y. Huang, S. He, W. Cao, K. Cai, X. Liang, *Nanoscale* **2012**, *4*, 6135-6149.
2. L. C. Kennedy, L. R. Bickford, N. A. Lewinski, A. J. Coughlin, Y. Hu, E. S. Day, J. L. West, R. A. Drezek, *Small* **2011**, *7*, 169-183.
3. X. Q. Zhang, X. Xu, R. Lam, D. Giljohann, D. Ho, C. A. Mirkin, *ACS Nano* **2011**, *5*, 6962-6970.
4. A. C. Anselmo, S. Mitragotri, *AAPS J* **2015**, *17*, 1041-1054.
5. X. Huang, I. H. El-Sayed, W. Qian, M. A. El-Sayed, *J. Am. Chem. Soc.* **2006**, *128*, 2115-2120.
6. Y. Cheng, J. D. Meyers, A. Broome, M. E. Kenney, J. P. Basilion, C. Burda, *J. Am. Chem. Soc.* **2011**, *133*, 2583-2591.
7. S. Jain, D. G. Hirst, J. M. O'Sullivan, *Brit. J. Radiol.* **2012**, *85*, 101-113.
8. R. A. Kudgus, R. Bhattacharya, P. Mukherjee, *Anticancer Agents Med. Chem.* **2011**, *11*, 965-973.
9. R. K. Delong, C. M. Reynolds, Y. Malcolm, A. Schaeffer, T. Severs, A. Wanekaya, *Nanotechnol. Sci. Appl.* **2010**, *3*, 53-63.
10. a) M. E. Gallina, Y. Zhou, C. J. Johnson, D. Harris-Birtill, M. Singh, H. Zhao, D. Ma, T. Cass, D. S. Elson, *Mater. Sci. Eng. C* **2016**, *59*, 324-332; b) P. K. Jain, X. Huang, I. H. El-Sayed, M. A. El-Sayed, *Acc. Chem. Res.* **2008**, *41*, 1578-1586; c) E. C. Dreaden, A. M. Alkilany, X. Huang, C. J. Murphy, M. A. El-Sayed, *Chem. Soc. Rev.* **2012**, *41*, 2740-2779.
11. a) P. Caravan, *Chem. Soc. Rev.* **2006**, *35*, 512-523; b) M. Botta, L. Tei, *Eur. J. Inorg. Chem.* **2012**, *2012*, 1945-1960.
12. a) G. J. Stasiuk, S. Tamang, D. Imbert, C. Gateau, P. H. Fries, P. Reiss, M. Mazzanti, *Dalton Trans.* **2013**, *42*, 8197-8200; b) G. J. Stasiuk, S. Tamang, D. Imbert, C. Poillot, M. Giardiello, C. Tisseyre, E. L. Barbier, P. H. Fries, M. de Waard, P. Reiss, M. Mazzanti, *ACS Nano* **2011**, *5*, 8193-8201; c) M. Filippi, D. Remotti, M. Botta, E. Terreno, L. Tei, *Chem. Commun.* **2015**, *51*, 17455-17458; d) N. A. Keasberry, M.



- Bañobre-López, C. Wood, G. J. Stasiuk, J. Gallo, N. J. Long, *Nanoscale* **2015**, *7*, 16119-16128; e) G. J. Stasiuk, N. J. Long, *Chem. Commun.* **2013**, *49*, 2732-2746.
13. M. F. Ferreira, B. Mousavi, P. M. Ferreira, C. I. O. Martins, L. Helm, J. A. Martins, C. F. G. C. Geraldès, *Dalton Trans.* **2012**, *41*, 5472-5475.
14. J. D. E. T. Wilton-Ely, *Dalton Trans.* **2008**, 25-29.
15. S. Sung, H. Holmes, L. Wainwright, A. Toscani, G. J. Stasiuk, A. J. P. White, J. D. Bell, J. D. E. T. Wilton-Ely, *Inorg. Chem.* **2014**, *53*, 1989-2005.
16. E. R. Knight, A. R. Cowley, G. Hogarth, J. D. E. T. Wilton-Ely, *Dalton Trans.* **2009**, 607-608.
17. E. R. Knight, N. H. Leung, Y. H. Lin, A. R. Cowley, D. J. Watkin, A. L. Thompson, G. Hogarth, J. D. E. T. Wilton-Ely, *Dalton Trans.* **2009**, 3688-3697.
18. V. L. Hurtubise, J. M. McArdle, S. Naeem, A. Toscani, A. J. P. White, N. J. Long, J. D. E. T. Wilton-Ely, *Inorg. Chem.* **2014**, *53*, 11740-11748.
19. E. R. Knight, N. H. Leung, A. L. Thompson, G. Hogarth, J. D. E. T. Wilton-Ely, *Inorg. Chem.* **2009**, *48*, 3866-3874.
20. Y. Zhao, W. Pérez-Segarra, Q. Shi, A. Wei, *J. Am. Chem. Soc.* **2005**, *127*, 7328-7329.
21. M. S. Vickers, J. Cookson, P. D. Beer, P. T. Bishop, B. Thiebaut, *J. Mater. Chem.* **2006**, *16*, 209-215.
22. S. Naeem, S. A. Serapian, A. Toscani, A. J. P. White, G. Hogarth, J. D. E. T. Wilton-Ely, *Inorg. Chem.* **2014**, *53*, 2404-2416.
23. P. D. Jadzinsky, G. Calero, C. J. Ackerson, D. A. Bushnell, R. D. Kornberg, *Science* **2007**, *318*, 430-433.
24. M. Friederici, I. Angurell, M. Seco, O. Rossell, J. Llorca, *Dalton Trans.* **2011**, *40*, 7934-7940.
25. G. J. Stasiuk, N. J. Long, *Chem. Commun.* **2013**, *49*, 2732-2746.
26. a) J. D. E. T. Wilton-Ely, D. Solanki, G. Hogarth, *Eur. J. Inorg. Chem.* **2005**, 4027-4030; b) E. R. Knight, D. Solanki, G. Hogarth, K. B. Holt, A. L. Thompson, J. D. E. T. Wilton-Ely, *Inorg. Chem.* **2008**, *47*, 9642-9653; c) E. R. Knight, N. H. Leung, A. L. Thompson, G. Hogarth, J. D. E. T. Wilton-Ely, *Inorg. Chem.* **2009**, *48*, 3866-3874; d) M. J. Macgregor, G. Hogarth, A. L. Thompson, J. D. E. T. Wilton-Ely, *Organometallics* **2009**, *28*, 197-208; e) G. Hogarth, E.-J. C.-R. C. R. Rainford-Brent, S. E. Kabir, I. Richards, J. D. E. T. Wilton-Ely, Q. Zhang, *Inorg. Chim. Acta* **2009**, *362*, 2020-2026; f) A. Toscani, E. K. Heliövaara, J. B. Hena, A. J. P. White, J. D. E. T. Wilton-Ely, *Organometallics* **2015**, *34*, 494-505; g) J. A. Robson, F. González de Rivera, K. A.

- Jantan, M. N. Wenzel, A. J. P. White, O. Rossell, J. D. E. T. Wilton-Ely, *Inorg. Chem.* **2016**, *55*, 12982-12996; h) A. Toscani, K. A. Jantan, J. B. Hena, J. A. Robson, E. J. Parmenter, V. Fiorini, A. J. P. White, S. Stagni, J. D. E. T. Wilton-Ely, *Dalton Trans.* **2017**, *46*, 5558-5570.
27. M. Ou, Y. Chen, Y. Chang, W. Lu, G. Liu, Y. Wang, *Dalton Trans.* **2007**, 2749-2759.
28. S. Laurent, L. Vander Elst, C. Henoumont, R. N. Muller, *Contrast Media Mol. Imaging* **2010**, *5*, 305-308.
29. A. J. Mieszawska, W. J. M. Mulder, Z. A. Fayad, D. P. Cormode, *Mol. Pharmaceutics* **2013**, *10*, 831-847.
30. Y. Song, X. Xu, K. W. MacRenaris, X. Zhang, C. A. Mirkin, T. J. Meade, *Angew. Chem. Int. Ed.* **2009**, *48*, 9143-9147.
31. M. D. Salazar, M. Ratnam, *Cancer Metastasis Rev.* **2007**, *26*, 141-152.
32. a) J. Park, W. I. Jeon, S. Y. Lee, K.-S. Ock, J. H. Seo, J. Park, E.-O. Ganbold, K. Cho, N. W. Song, S.-W. Joo, *J. Biomed. Mater. Res. Part A* **2012**, *100A*, 1221-1228; b) A. R. Vortherms, R. P. Doyle, D. Gao, O. Debrah, P. J. Sinko, *Nucleosides Nucleotides Nucleic Acids* **2008**, *27*, 173-185; c) A. Gabizon, A. T. Horowitz, D. Goren, D. Tzemach, F. Mandelbaum-Shavit, M. M. Qazenand, S. Zalipsky, *Bioconjugate Chem.* **1999**, *10*, 289-298; d) C. P. Leamon, P. S. Low, *PNAS* **1991**, *88*, 5572-5576.
33. F. Geng, K. Song, J. Z. Xing, C. Yuan, S. Yan, Q. Yang, J. Chen, B. Kong, *Nanotechnology* **2011**, *22*, 285101.
34. M. Marradi, D. Alcántara, J. Martínez de la Fuente, M. L. García-Martín, S. Cerdán, S. Penadés, *Chem. Commun.* **2009**, 3922-3924.
35. T. Kowada, H. Maeda, K. Kikuchi, *Chem. Soc. Rev.* **2015**, *44*, 4953-4972.
36. a) C. Alric, J. Taleb, G. Le Duc, C. Mandon, C. Billotey, A. Le Meur-Herland, T. Brochard, F. Vocanson, M. Janier, P. Perriat, S. Roux, O. Tillement, *J. Am. Chem. Soc.* **2008**, *130*, 5908-5915; b) L. Moriggi, C. Cannizzo, E. Dumas, C. R. Mayer, A. Ulianov, L. Helm, *J. Am. Chem. Soc.* **2009**, *131*, 10828-10829.
37. a) A. Irure, M. Marradi, B. Arnáiz, N. Genicio, D. Padroc, S. Penadés, *Biomater. Sci.* **2013**, *1*, 658-668; b) F. J. Nicholls, M. W. Rotz, H. Ghuman, K. W. MacRenaris, T. J. Meade, M. Modo, *Biomaterials* **2016**, *77*, 291-306; c) R. J. Holbrook, N. Rammohan, M. W. Rotz, K. W. MacRenaris, A. T. Preslar, T. J. Meade, *Nano Lett.* **2016**, *16*, 3202-3209; d) N. Rammohan, R. J. Holbrook, M. W. Rotz, K. W. MacRenaris, A. T. Preslar, C. E. Carney, V. Reichova, T. J. Meade, *Bioconjugate Chem.* **2017**, *28*, 153-160; e) C. Zeng, X. Shi, B. Wu, D. Zhang, W. Zhang, *Colloids Surfaces B Biointerfaces* **2014**,

123, 130-135; f) V. S. Marangoni, O. Neumann, L. Henderson, C. C. Kaffes, H. Zhang, R. Zhang, S. Bishnoi, C. Ayala-Orozco, V. Zucolotto, J. A. Bankson, P. Nordlander, N. J. Halas, *Proc. Natl. Acad. Sci. U. S. A.* **2017**, *114*, 6960-6965; g) G. Liang, L. Xiao, *Biomater. Sci.* **2017**, *5*, 2122-2130; h) Y. Zeng, D. Zhang, M. Wu, Y. Liu, X. Zhang, L. Li, Z. Li, X. Han, X. Wei, X. Liu, *ACS Appl. Mater. Interfaces* **2014**, *6*, 14266-14277; i) Q. Chen, H. Wang, H. Liu, S. Wen, C. Peng, M. Shen, G. Zhang, X. Shi, *Anal. Chem.* **2015**, *87*, 3949-3956; j) B. Zhou, Z. Xiong, J. Zhu, M. Shen, G. Tang, C. Peng, X. Shi, *Nanomedicine* **2016**, *11*, 1639-1652; k) K. S. B. Culver, Y. J. Shin, M. W. Rotz, T. J. Meade, M. C. Hersam, T. W. Odom, *J. Phys. Chem. C* **2016**, *120*, 22103-22109; l) L. F. Vistain, M. W. Rotz, R. Rathore, A. T. Preslar, T. J. Meade, *Chem. Commun.* **2016**, *52*, 160-163; m) B. Zhou, Z. Xiong, P. Wang, C. Peng, M. Shen, S. Mignani, J.-P. Majoral, X. Shi, *Drug Deliv.* **2018**, *25*, 178-186; n) V. Mogilireddy, I. Déchamps-Olivier, C. Alric, G. Laurent, S. Laurent, L. Vander Elst, R. Muller, R. Bazzi, S. Roux, O. Tillement, F. Chuburu, *Contrast Media Mol. Imaging* **2015**, *10*, 179-187; o) A. Pitchaimani, T. D. T. Nguyen, L. Maurmann, J. Key, S. H. Bossmann, S. Aryal, *J. Biomed. Nanotechnol.* **2017**, *13*, 417-426; p) C. Zeng, X. Shi, B. Wu, D. Zhang, W. Zhang, *Colloids Surfaces B Biointerfaces* **2014**, *123*, 130-135; q) V. S. Marangoni, O. Neumann, L. Henderson, C. C. Kaffes, H. Zhang, R. Zhang, S. Bishnoi, C. Ayala-Orozco, V. Zucolotto, J. A. Bankson, P. Nordlander, N. J. Halas, *Proc. Natl. Acad. Sci. U. S. A.* **2017**, *114*, 6960-6965; r) G. Liang, L. Xiao, *Biomater. Sci.* **2017**, *5*, 2122-2130; s) Y. Zeng, D. Zhang, M. Wu, Y. Liu, X. Zhang, L. Li, Z. Li, X. Han, X. Wei, X. Liu, *ACS Appl. Mater. Interfaces* **2014**, *6*, 14266-14277; t) Q. Chen, H. Wang, H. Liu, S. Wen, C. Peng, M. Shen, G. Zhang, X. Shi, *Anal. Chem.* **2015**, *87*, 3949-3956; u) B. Zhou, Z. Xiong, J. Zhu, M. Shen, G. Tang, C. Peng, X. Shi, *Nanomedicine* **2016**, *11*, 1639-1652; v) K. S. B. Culver, Y. J. Shin, M. W. Rotz, T. J. Meade, M. C. Hersam, T. W. Odom, *J. Phys. Chem. C* **2016**, *120*, 22103-22109; w) L. F. Vistain, M. W. Rotz, R. Rathore, A. T. Preslar, T. J. Meade, *Chem. Commun.* **2016**, *52*, 160-163; x) B. Zhou, Z. Xiong, P. Wang, C. Peng, M. Shen, S. Mignani, J.-P. Majoral, X. Shi, *Drug Deliv.* **2018**, *25*, 178-186; y) V. Mogilireddy, I. Déchamps-Olivier, C. Alric, G. Laurent, S. Laurent, L. Vander Elst, R. Muller, R. Bazzi, S. Roux, O. Tillement, F. Chuburu, *Contrast Media Mol. Imaging* **2015**, *10*, 179-187; z) A. Pitchaimani, T. D. T. Nguyen, L. Maurmann, J. Key, S. H. Bossmann, S. Aryal, *J. Biomed. Nanotechnol.* **2017**, *13*, 417-426.

38. J. M. Wessels, H.-G. Nothofer, W. E. Ford, F. von Wrochem, F. Scholz, T. Vossmeier, A. Schroedter, H. Weller, A. Yasuda, *J. Am. Chem. Soc.* **2004**, *126*, 3349-3356.
39. a) T. B. Huff, M. N. Hansen, Y. Zhao, J.-X. Cheng, A. Wei, *Langmuir* **2007**, *23*, 1596-1599; b) M.-H. Park, Y. Ofir, B. Samanta, P. Arumugam, O. R. Miranda, V. M. Rotello, *Adv. Mat.* **2008**, *20*, 4185-4188; c) M. N. Hansen, L.-S. Chang, A. Wei, *Supramol. Chem.* **2008**, *20*, 35-40; d) D. P. Cormode, J. J. Davis, P. D. Beer, *J. Inorg. Organomet. Polym.* **2008**, *18*, 32-40; e) J. Sharma, R. Chhabra, H. Yan, Y. Liu, *Chem. Commun.* **2008**, 2140-2142; f) H. Zhu, D. M. Coleman, C. J. Dehen, I. M. Geisler, D. Zemlyanov, J. Chmielewski, G. J. Simpson, A. Wei, *Langmuir* **2008**, *24*, 8660-8666; g) C. Subramani, Y. Ofir, D. Patra, B. J. Jordan, I. W. Moran, M.-H. Park, K. R. Carter, V. M. Rotello, *Adv. Funct. Mater.* **2009**, *19*, 2937-2942; h) M.-H. Park, Y. Ofir, B. Samanta, V. M. Rotello, *Adv. Mat.* **2009**, *21*, 2323-2327; i) H. Ichikawa, K. Yasui, M. Ozawa, K. Fujita, *Synth. Metals* **2009**, *159*, 973-976; j) G. Patel, A. Kumar, U. Pal, S. Menou, *Chem. Commun.* **2009**, 1849-1851; k) H. Wan, L. Chen, J. Chen, H. Zhou, L. Liu, *J. Dispersion Sci. Technol.* **2009**, *30*, 194-197; l) Y. Zhao, J. N. Newton, J. Liu, A. Wei, *Langmuir* **2009**, *25*, 13833-13839; m) C. Subramani, A. Bajaj, O. R. Miranda, V. M. Rotello, *Adv. Mat.* **2010**, *22*, 5420-5423; n) X. Duan, M.-H. Park, Y. Zhao, E. Berenschot, Z. Wang, D. N. Reinhoudt, V. M. Rotello, J. Huskens, *ACS Nano* **2010**, *4*, 7660-7666; o) M. H. Park, X. X. Duan, Y. Ofir, B. Creran, D. Patra, X. Y. Ling, J. Huskens, V. M. Rotello, *ACS Appl. Mater. Interf.* **2010**, *2*, 795-799; p) M.-H. Park, S. S. Agasti, B. Creran, C. Kim, V. M. Rotello, *Adv. Mat.* **2011**, *23*, 2839-2842; q) K. Chen, H. D. Robinson, *J. Nanopart. Res.* **2011**, *13*, 751-761; r) F. Wrochem, D. Gao, F. Scholz, H. Nothofer, G. Nelles, J. Wessels, *Nat. Nanotechnol.* **2010**, *119*, 1-7.
40. I.-C. Yoon, K. Karlssons, F. Bresme, J. D. E. T. Wilton-Ely, unpublished results.
41. M. Brust, J. Fink, D. Bethell, D. J. Schiffrin, C. Kiely, *J. Chem. Soc., Chem. Commun.* **1995**, 1655-1656.
42. Following the method used by D. J. Lewis, T. M. Day, J. V. MacPherson, Z. Pikramenou, *Chem. Commun.* **2006**, 1433-1435.
43. M. Yamagata, Y. Okamoto, Y. Akiyama, H. Takahashi, T. Kawano, Y. Katayama, Y. Niidome, *J. Controlled Release* **2006**, *114*, 343-347.
44. a) P.-J. Debouttière, S. Roux, F. Vocanson, C. Billotey, O. Beuf, A. Favre-Réguillon, Y. Lin, S. Pellet-Rostaing, R. Lamartine, P. Perriat, O. Tillement, *Adv. Funct. Mater.* **2006**, *16*, 2330-2339; b) M. Milne, P. Gobbo, N. McVicar, R. Bartha, M. S. Workentin, R. H. E. Hudson, *J. Mater. Chem. B* **2013**, *1*, 5628-5635; c) D. Y. Joh, L. Sun, M.

- Stangl, A. Al Zaki, S. Murty, P. P. Santoiemma, J. J. Davis, B. C. Baumann, M. Alonso-Basanta, D. Bhang, G. D. Kao, A. Tsourkas, J. F. Dorsey, *PLoS One* **2013**, *8*, e62425; d) M. F. Ferreira, J. Gonçalves, B. Mousavi, M. I. M. Prata, S. P. J. Rodrigues, D. Calle, P. López-Larrubia, S. Cerdan, T. B. Rodrigues, P. M. Ferreira, L. Helm, J. A. Martins, C. F. G. C. Geraldés, *Dalton Trans.* **2015**, *44*, 4016-4031; e) J.-A. Park, P. A. N. Reddy, H.-K. Kim, I.-S. Kim, G.-C. Kim, Y. Chang, T.-J. Kim, *Bioorg. Med. Chem. Lett.* **2008**, *18*, 6135-6137.
45. M. F. Warsi, V. Chechik, *PCCP* **2011**, *13*, 9812-9817.
46. A. Irure, M. Marradi, B. Arnáiz, N. Genicio, D. Padro, S. Penadés, *Biomater. Sci.* **2013**, *1*, 658-668.
47. C. Morelli, P. Maris, D. Sisci, E. Perrotta, E. Brunelli, I. Perrotta, M. L. Panno, A. Tagarelli, C. Versace, M. F. Casula, F. Testa, S. Ando, J. B. Nagya, L. Pasqua, *Nanoscale* **2011**, *3*, 3198-3207.
48. H. Jo, J. Her, C. Ban, *Biosens. Bioelectron.* **2015**, *71*, 129-136.
49. G. P. Acuna, M. Bucher, I. H. Stein, C. Steinhauer, A. Kuzyk, P. Holzmeister, R. Schreiber, A. Moroz, F. D. Stefani, T. Liedl, F. C. Simmel, P. Tinnefeld, *ACS Nano* **2012**, *6*, 3189-3195.